

On-wafer photoacid determination and imaging technique for chemically amplified photoresists

Paul M. Dentinger,^{a)} Bing Lu, and James W. Taylor^{b)}
Center for X-ray Lithography, University of Wisconsin-Madison, Stoughton, Wisconsin 53589-3097

Scott J. Bukofsky,^{c)} Gilbert D. Feke, Dan Hessman, and Robert D. Grober
Department of Applied Physics, Yale University, New Haven, Connecticut 06520-8284

(Received 29 May 1998; accepted 14 September 1998)

A fundamental task of chemically amplified photoresists is to record the incident radiation by generating catalyst concentration gradients within the film. In many resists, the catalyst is a strong Brønsted acid which yields a latent image of pH within the exposed film. A number of mechanistic questions remain about acid generator efficiency and its mobility once generated and heated. We have developed a technique in which a pH -dependent fluorophore is incorporated into the resist (an undyed version of SAL 605 from the Shipley Company and similar formulations). The localized acid concentrations generated by exposure to x-rays are analyzed and imaged using fluorescence spectroscopy and microscopy. Initial experiments, the spectroscopic apparatus, and initial far-field imaging are reported elsewhere [S. J. Bukofsky, G. D. Feke, Q. Wu, R. D. Grober, P. M. Dentinger, and J. W. Taylor, *Appl. Phys. Lett.* **73**, 3 (1998)]. In this article, several fluorophores are evaluated, and various criteria for successful imaging within the photoresist matrix are established. These criteria include pK_a of the fluorophore, photostability, and functional groups that affect the performance of the acid within the film. The technique is used to show the relative efficiency of two photoacid generators in otherwise identical matrices, and the method has the potential for rapid photogenerated acid yield determination among a variety of photoacid generators. This technique can be used in thin imaging films and, due to the low level of fluorophore required (0.01–0.1 wt. %), for photoacid yield determination in optical photoresists without significantly altering the absorbance characteristics of the film. Initial near-field scanning optical microscopy images are shown and the potential of the technique for several lithographic applications, including measurement of the actual spread of the acid distribution during postexposure bake, is discussed.
© 1998 American Vacuum Society. [S0734-211X(98)08406-6]

I. INTRODUCTION

The performance of the photoacid generator (PAG) during exposure and the photogenerated acid during postexposure bake (PEB) delay as well as the PEB itself is one of the critical parameters in the success of chemically amplified resists. An analytical technique for determining photoacid concentration and distribution in the matrix of the film would be a significant addition to our ability to map the response of these chemically amplified resist materials. While spectrophotometric titration has been utilized by a number of authors,^{1–4} and even spectrofluorometric titration^{5–8} has been used to quantify the amount of acid, these are destructive techniques which ultimately are not performed in the same matrix as the lithography step. In addition, nearly an entire wafer must be blanketed with radiation in order to generate enough acid to give the sensitivity needed to perform the analysis. This does not allow measurements to be made in small exposure field systems and it is difficult with direct-write electron beam exposure. In addition, experimental verification of the spatially resolved acid distribution is not possible with these titration techniques. One can only determine

the acid concentration versus dose via titration, and then use models of incident dose distribution to correlate initial acid distribution within the film.

Fluorescent molecules excited within polymers have been utilized extensively in the biological community. However, biological polymers are often measured at near-neutral pH in aqueous environments, mimicking biologically relevant conditions. It may not be possible to introduce an aqueous environment to practical photoresists and expect the same response of the photoresist as that under lithographic conditions. For example, airborne water has been identified as a major contamination source for negative-tone, chemically amplified resists,^{9,10} and airborne base contamination on the order of parts per billion has been identified as problematic for positive-tone systems.¹¹ Pohlers *et al.* have achieved photoactivated, pH -dependent fluorescent spectra within polymer films.^{7,8} However, pH -dependent spectra for rhodamine B and fluorescein were collected only in films of polymethylmethacrylate (PMMA) as they concluded that the lactone ring was opened in polyvinylphenol (PVP) for these dyes. Photoresist materials are defined by imaging performance, and an on-wafer acid measurement technique is limited to the matrix (resist) and conditions under which lithography occurs.

SAL 605 was chosen for latent image acid determination.

^{a)}Present address: Sandia National Laboratories, Livermore, CA.

^{b)}Electronic mail: jwtaylor@xraylith.wisc.edu

^{c)}Present address: IBM Corp., Hopewell Junction, NY.

This is a negative-tone, e-beam/x-ray resist based on a novolac resin, hexamethoxymethylmelamine (HMMM), and a PAG.¹² The acid concentration generated upon exposure to x-rays from the ES-5 beam line at the Center for X-ray Lithography (CXrL) at the University of Wisconsin–Madison has been quantified by spectrophotometric titration,¹³ and the processing conditions are well developed at CXrL. The PEB delay time stability for this experiment is important because the exposures were done at the University of Wisconsin and the fluorescence measurements were done at Yale (New Haven, CT). The PEB delay time stability has been measured by infrared absorption peak height formation by Gamsky *et al.*¹⁴ to be roughly 24 h for 1 μm thick films, by dose to size by Fedynshyn *et al.* for SAL 603 under e-beam exposure to be approximately 24 (Ref. 15) and approximately 12 h for 0.5 μm thick films in an open cleanroom, as measured by real-time Fourier transform infrared (RT-FTIR) kinetics.¹⁶ However, the source of the delay instability of these novolac-based chemically amplified resists is known to be airborne water contamination, and film life has been increased to weeks by storing the coated films under dry conditions.^{9,17} Therefore, removing humidity from the storage environment should improve the PEB delay stability to longer than 12 h. In addition, if the failure mode is predominantly from attack of the melamine crosslinker by water, and not scavenging of the acid as found in positive-tone systems, we expect that this technique, which measures acid concentration, may not be particularly susceptible to delay times, at least on the order of 24 h.

The essential aspects of near-field scanning optical microscopy (NSOM) are as follows. Light is guided along a single-mode optical fiber, and exits through an aperture approximately 70 nm in diameter. The aperture is formed by chemically etching the optical fiber into a sharp tip¹⁸ and metallizing the outer wall by shadow evaporation. The fiber probe acts as a local illumination source, and operates in close proximity (10–50 nm) to the sample. The spatial resolution of this system is approximately equivalent to the near-field aperture diameter, about 70 nm.

In this article, some general aspects of fluorescence from photoresist films are shown. We show the utility of the on-wafer spectrofluorometric titration technique to evaluate the relative efficiency of PAGs in the matrix of the lithographic process. In addition, fluorescence imaging is used, and an initial comparison of near-field and far-field imaging is discussed. The potential of this technique for accurately determining the movement of acid during the PEB is also discussed.

II. EXPERIMENT

Fluorescent probes Cl-NERF and Cl₂TFF were purchased from Molecular Probes (Eugene, OR). The photoacid generators, tetrabromobisphenol A (TBBPA) and tetrachlorobisphenol A (TCBPA), were obtained from Aldrich (Milwaukee, WI). All were used as received, and the structures are shown in Fig. 1. Novolac resin was obtained from Schenectady International (Schenectady, NY) and the HMMM

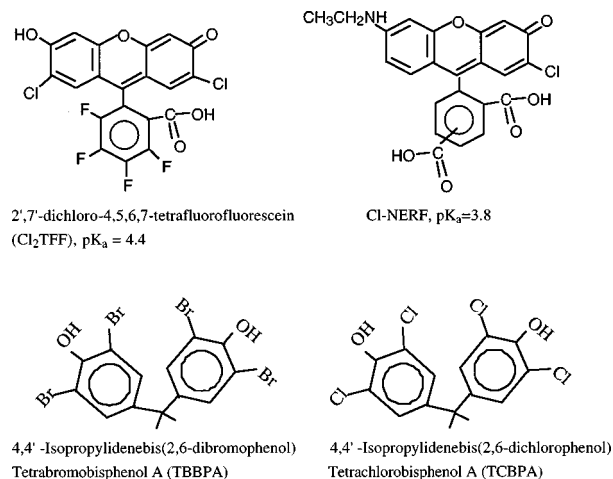


FIG. 1. Top: Fluorescent probes investigated in this study. Bottom: Photoacid generators used in this study.

product, Cymel 300 (American Cyanamid, Wayne, NJ), was obtained and used as received. All wt. % additives are reported versus solids content of the casting solution. A formulation of SAL 605 which did not contain the visual contrast enhancing dye was graciously donated by The Shipley Co. The molecular probes were added to SAL 605 casting solution and similar formulations and were spun onto visually transparent soda-lime wafers. These films were processed with a postapply bake of 118 °C, for 72 s. Exposures were made at the CXrL on the ES-5 beamline connected to a Karl Suss XRS 200/2M x-ray stepper, unless stated otherwise. Blanket exposure doses on this beamline are reported as to a 2 μm silicon nitride membrane. The membrane absorbs approximately 50% of the radiation at these wavelengths. Patterned exposures were through an IBM LT 25 mask which employs approximately 0.6 μm of Au absorber and absorbs roughly 90% of the radiation at these wavelengths. When a PEB was applied, the conditions were 108 °C for 60 s. The exposed wafers were placed in a wafer box packed with approximately 10 g of molecular sieves (5 g each of 5 Å, Union Carbide, Plainfield, NJ, and 4 Å, Matheson Coleman, Norwood, OH), outgassed with dry nitrogen, and sealed before shipment to Yale University. Typical exposures were done in the afternoon, and the wafers were received at Yale by 10:30 am the next day. The delay time for the dry storage conditions was thus between 16 and 20 h. Ultraviolet visible (UV-vis) spectra were measured at CXrL with a Hewlett-Packard 8452 apparatus. RT-FTIR spectroscopy for kinetics measurements was performed as discussed in a prior publication.¹⁹

Fluorescence excitation at Yale was performed using the 514 nm line of an Ar-ion laser. The photons collected were those whose wavelengths were greater than 10 nm from the exciting beam. Details of the far-field imaging are in a prior publication.²⁰ The near-field images were formed by rastering the sample through the pump beam provided by the near-field probe, and collecting photons in the far field. Fluorescence was collected with a 0.8 numerical aperture (NA), 100 \times microscope objective, and imaged onto an avalanche photodiode (APD). Two holographic notch filters (Kaiser

Corp.) were used to remove the pump beam from the detector. The dark count on the APD was less than 50 counts/s, and the fluorescence during imaging was orders of magnitude greater than this, allowing high signal to noise ratios. It is also important to mention that these NSOM experiments using molecular fluorescence as an imaging source are made possible by the increased optical throughput of chemically etched fiber probes.¹⁸

III. RESULTS AND DISCUSSION

A. Defining the fluorophore and matrix

Initial experiments were performed to determine the range of pH for which a fluorophore incorporated within the SAL 605 matrix would need to be sensitive. First, the effective pH of the film was estimated by incorporating several pH -sensitive dyes into the film and measuring their UV-vis absorption spectra to determine if they were predominantly in their acidic or basic form. Tetrabromophenol blue sodium salt, Congo Red, and Bromocresol Green were incorporated into the film at 1 wt. % and measured. From the resulting spectra, and the known pK_a 's of these dyes in water, an "effective" pH of the film was estimated to be approximately 4.0–4.5.²¹ Under x-ray exposure sufficient for imaging, this resist generates approximately 5×10^{-6} moles H^+ /cm³.¹³ If we assume that the acid is completely dissociated, then the pH drops from approximately 4.3 to 2.3. Thus, one would prefer to have a fluorophore with pK_a of effectively 3.4 in the SAL 605 matrix. There is a variety of pH -dependent fluorophores that meet this criterion, such as tetrachloro-tetrabromo fluorescein and tetraiodo fluorescein. We found that incorporation of brominated dyes into photoresist matrices will result in a change in absorbance purely from the photolytic decomposition of the dye itself as was shown elsewhere.²² Presumably, the iodinated fluorophore would have similar restrictions when using x-ray radiation. It is also important that the sensing dye itself not interfere with the measurement. Using pH -sensitive fluorophores like *o*-phenylene diamine would cause concern because of the high levels of primary amines incorporated into the film with this fluorophore, which would presumably alter the measurement of the activity of the generated acid, as will be discussed in Sec. III D. Nonetheless, use of *o*-phenylene diamine was attempted because of the desirable property that it increases fluorescence with decreasing pH .²³ However, this fluorophore photobleached rapidly and was not useful for analysis. Therefore, the fluorophores shown in Fig. 1 were chosen.

The UV-vis absorption spectra of the two fluorophores in undyed SAL 605 as well as the undyed SAL 605 matrix are shown in Fig. 2. The Cl-NERF fluorophore is a hybrid of fluorescein and rhodamine dyes with the added electron-withdrawing group to lower its pK_a to 3.8, and whose fluorescence excitation is quenched with decreasing pH .²⁴ Figure 2 shows that Cl-NERF in SAL 605 has a reasonably high ratio of absorbance at 530 nm to that at 490 nm, indicative of the dye in its basic or near- pK_a environment.²⁵ However, the ratio of the peaks for the Cl₂TFF is quite small,

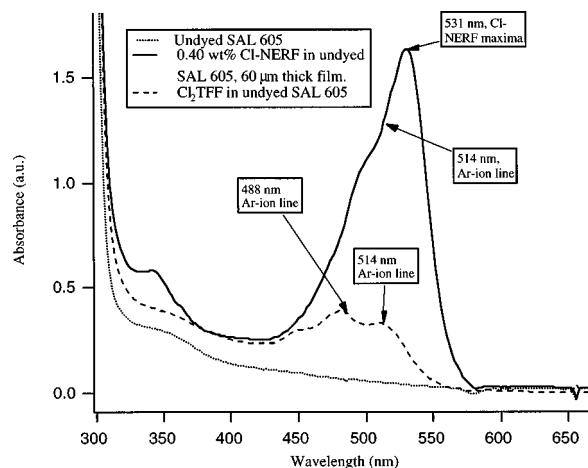


FIG. 2. UV-vis spectrum of fluorophores used in this study in the undyed SAL 605 matrix.

indicative of the probe in an environment with pH below its pK_a of 4.4 (in water). Subsequent fluorescence experiments showed approximately an order of magnitude less fluorescence from the Cl₂TFF molecule in the undyed SAL 605 matrix, again indicative that its pK_a is too high for the experiment. This is consistent with the estimated effective pH of the medium. In general, fundamental considerations of pH and pK_a which were defined for water, appeared to hold up in the SAL 605 matrix for the fluorescent probes investigated here. Cl-NERF was then chosen for subsequent experiments, and showed a linear increase in fluorescence with the wt. % fluorophore added up to approximately 0.15 wt. %, as shown previously,²⁰ where presumably self-quenching began to occur at the higher level. For this work, a concentration of 0.07 wt. % was used. In addition, the visual contrast enhancing dye in SAL 605 appeared to decrease the fluorescence yield by roughly a factor of 2, and hence the undyed version was used.

B. Comparison of on-wafer spectrofluorometric titration of photoacid generators

One application of the on-wafer acid determination technique is to test the efficiency of photoacid generators in the matrix of lithographic conditions. In this experiment, in-house formulations of novolac and HMMM were prepared with the added photoacid generators TBBPA and TCBPA and 0.07 wt. % of Cl-NERF fluorophore. The films were spun to 0.5 μm thickness, and exposed on the ES-1 beamline without a silicon nitride membrane. Figure 3 shows the results of the experiment. The fluorescence decreased monotonically with increased dose. It is important to note that films without photoacid generators did not show fluorescent images up to doses of 600 mJ/cm² to a SiN membrane, indicating that the drop in fluorescence due to exposure was predominantly due to the generation of acid, not due to the photodecomposition of the fluorophore. In this experiment, it appeared as if the fluorescence were decreased roughly 33% more efficiently, by mass, with the chlorine-containing PAG.

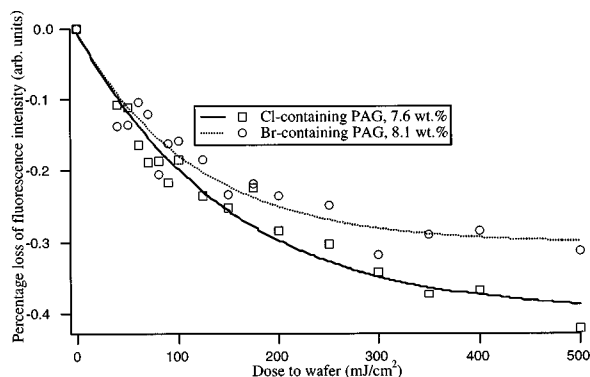


FIG. 3. Comparison of on-wafer spectrofluorometric titration of films with two different PAGs. The chlorine-containing PAG, TCBPA, appears to generate more acid per unit mass.

However, because the molecular weight of TCBPA is about 33% less than that of the TBBPA, it is likely that the apparent higher efficiency of TCBPA can be attributed to the additional moles of TCBPA PAG in the film. Normalized remaining thickness (NRT) curves were also obtained for these two formulations and they corroborated the results. The film containing TCBPA was approximately two times more sensitive, as measured by the NRT of developed pads, than the film with TBBPA, although there were some effects of PAG on contrast. This result underscores the utility of this technique; the ability to measure the efficiency of the acid generation process without interference of kinetics, volatility, dissolution behavior, etc., which can confound results when developed features are used as the detector.

C. Imaging of photogenerated acid

It was shown above that the presence of acid can alter the fluorescence of the film if the appropriate probe is added. Here in Sec. III C, the films are exposed to x-rays through a mask and fluorescence imaging is used to spatially resolve the acid concentration. Figure 4 shows the results of these experiments. Fluorescence images are shown in Figs. 4(a)–4(d) and a scanning electron micrograph (SEM) of the developed features in SAL 605 exposed through this mask is included in Fig. 4(e). There are several important results shown in Fig. 4. First, features in the latent image which correspond to the $0.25\ \mu\text{m}$ features on the mask are partially resolved by far-field imaging. However, the spot size of this far-field experiment is approximately $400\ \text{nm}$. This large spot size would likely preclude quantifying the spread of the acid images during PEB, a step necessary to make an accurate assessment of the acid mobility. Also, the optical contrast for the larger features on the mask was slightly higher than it was for the thin lines. There are several possible explanations for this: diffraction from the mask at a $25\ \mu\text{m}$ gap decreases the peak power at the center of the smallest lines during exposure with x-rays, the diffraction limited ($\approx 400\ \text{nm}$) spot size of the imaging apparatus could not completely resolve these lines, or a small amount of room temperature acid diffusion could be depleting the acid in the center of the $0.25\ \mu\text{m}$ lines. Another observation of importance was that

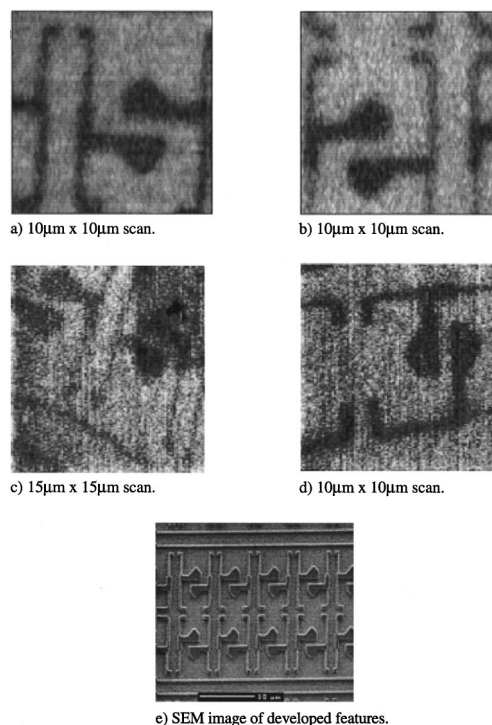


FIG. 4. Images of the dose delivered through a mask. (a) Fluorescent image with far-field excitation and no PEB. The film thickness was $500\ \text{nm}$ and the dose was $350\ \text{mJ}/\text{cm}^2$. (b) Same as (a), but with a PEB. (c) Fluorescent image with near-field excitation and no PEB. The film thickness was $150\ \text{nm}$ and the dose was $700\ \text{mJ}/\text{cm}^2$. (d) Same as (c) except with a PEB. (e) SEM of the developed images in SAL 605 with this mask at $125\ \text{mJ}/\text{cm}^2$. The minimum feature size on the mask is $0.25\ \mu\text{m}$.

the images without PEB [Fig. 4(a)] had lower contrast than those with a PEB [Fig. 4(b)]. The gray scales in Figs. 4(a) and 4(b) are not the same, but the contrast for the sample in Fig. 4(a) was 15% and the contrast for Fig. 4(b) was 30%. There are several possible explanations for this. The first is that the acid quickly forms a complex with the HMMM at room temperature and is liberated with the heat of the PEB, a process which has been invoked to explain the unusual PEB delay stability of these resists.²⁶ The second possibility is that the HMMM reacts with one or more of the functionalities of the fluorophore and the fluorescence is decreased by this reaction.

NSOM imaging in films of $150\ \text{nm}$ thickness is shown in Figs. 4(c) and 4(d). The images were acquired at 75 pixels/s. It should be noted that the advantage of using these chemically etched fiber probes is that they deliver enough illumination power to make images at rates comparable to that of the far field.¹⁸ The darkened square in the upper right corner of Fig. 4(c) is the result of photobleaching from a previous scan. Because the rhodol derivatives such as CI-NERF show higher photostability, in general, than fluorescein-based probes,²⁵ and because of the difficulty of using the *o*-phenylene diamine probe discussed above, this image underscores the importance of selecting high photostability fluorescent probes. Again, the baked images showed better contrast. In this near-field experiment, the aperture is roughly

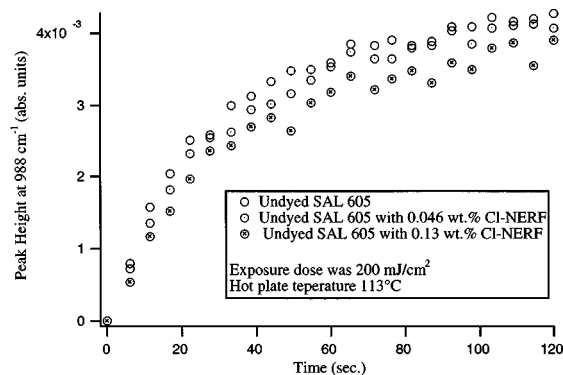


Fig. 5. RT-FTIR of the linking kinetics of HMMM and novolac in SAL 605 with the addition of the CI-NERF fluorescent probe. The probe appears to affect the reaction slightly.

70 nm, so the fluorescence imaging spot size is less than the minimum feature size of 250 nm on the mask, in contrast to the far-field images where the fluorescence imaging spot size was approximately 400 nm. The full width at half maximum (FWHM) of NSOM images of the thinnest features of the sample with the PEB was roughly 575 nm, between 16 and 20 h after exposure. This is significantly larger than the mask feature size. In addition to the acid distribution spreading during PEB, this could be due to the high dose used in this particular experiment. If the delivered dose distribution was Gaussian and the response of the fluorescence with dose was linear, one would not expect the FWHM to change with dose. However, the decrease in fluorescence with dose is not linear in this range. From Fig. 3, we see that the fluorescence becomes nonlinear at roughly a 150–200 mJ/cm² dose to the wafer on the ES-5 beamline. Because of absorption of the mask membrane of approximately 50%, membrane not used in Fig. 3, this corresponds to roughly 300–400 mJ/cm² to the mask. For the experiment in Fig. 4(d), the dose was 700 mJ/cm², so fluorescence was not linear with dose. Also, there could be some small component of room temperature acid diffusion over this time frame. However, the near-field apparatus is capable of achieving a smaller illumination size than the minimum mask feature size of 250 nm with data acquisition as similar rates to the far-field images, and these initial experiments set conditions which can be used for experiments in progress to utilize the sub-100 nm resolution capabilities of NSOM.

D. Potential for accurate diffusion coefficient measurement

The potential of NSOM to accurately determine the spread of the photogenerated acid distribution within the matrix of the photoresist depends on several factors. One of these factors is that the addition of the fluorophore to the film not affect the activity of the acid. The secondary amine on the CI-NERF molecule was suspected to affect the activity of the acid during the PEB. To test this, RT-FTIR spectroscopy of the kinetics of the linking reaction in the presence of the fluorophore CI-NERF was employed. Figure 5 shows the result of this experiment. Figure 5 shows that the addition of

CI-NERF does affect the kinetics of the reaction slightly. One explanation for this result is that the acid is “trapped” by the secondary amine on the fluorophore, and hence is less active. In addition, the HMMM could be reacting with the CI-NERF molecule, and creating a peak in the infrared spectrum which is not detected at 988 cm⁻¹, the peak of interest in the kinetics measurement. While there was no detectable difference in the IR spectra between the film without fluorophore and the film with fluorophore, this is not surprising because of the low concentration of the fluorophore. This latter explanation could explain why there is higher optical contrast in the images with a PEB than without, as shown in Fig. 4. The kinetics of ether formation does appear to be slightly affected by the presence of the probe. Potentially, this may be mitigated by moving to positive-tone systems which act by deprotection of otherwise aqueous-base soluble resins so that the possible reaction of the crosslinker with the fluorophore is avoided. Additionally, the use of high photostability fluorophores with the requisite pK_a and no amines may be useful.

IV. CONCLUSIONS

On-wafer fluorescence techniques were developed and used to monitor photoacid production. Conditions under which fluorescence techniques could be done in photoresist films were defined, and fundamental considerations of pH and pK_a defined for water appeared to hold for the fluorescent probes within the film as well. The on-wafer fluorescence techniques offer several important advantages over absorption techniques: they are fast, nondestructive, can be done in very thin films and on small area exposures, and ultimately done in nearly the same matrix as lithography. Far-field and near-field optical images were produced. Near-field imaging appeared to have the resolution required for an accurate measurement of the spread of the acid distribution during PEB, but several issues involving the interaction between the acid, the reacting species within the film, and the probing fluorophore need to be addressed, and they will be the subject of future work.

ACKNOWLEDGMENTS

This work was supported by Semiconductor Research Corporation Grant Nos. 98-LP-452 and 96-LJ-438. CXrL is supported by DARPA/ONR Grant No. N-00014-97-1-0460 and the Synchrotron Radiation Center is supported by the National Science Foundation under Grant No. DMR-95-31009. Two of the authors (P.M.D. and S.J.B.) acknowledge financial support from SRC fellowships.

¹D. R. McKean, U. Schaedeli, and S. A. MacDonald, *Polymers for Microlithography* (American Chemical Society, Washington, DC, 1989), pp. 27–38.

²T. H. Fedynyshyn, J. W. Thackeray, J. H. Georger, and M. D. Denison, *J. Vac. Sci. Technol. B* **12**, 3888 (1994).

³P. M. Dentinger, C. M. Nelson, S. J. Rhyner, J. W. Taylor, T. H. Fedynyshyn, and M. F. Cronin, *J. Vac. Sci. Technol. B* **14**, 4239 (1996).

⁴T. Itani, H. Yoshino, S. Hashimoto, M. Yamana, N. Samoto, and K. Kasama, *J. Vac. Sci. Technol. B* **14**, 4226 (1996).

⁵A. R. Eckert and W. M. Moreau, *Proc. SPIE* **3049**, 879 (1997).

- ⁶U. Okoroanyanwu, J. D. Byers, T. Cao, S. E. Webber, and C. G. Willson, *Proc. SPIE* **3333**, 747 (1998).
- ⁷G. Pohlers, S. Virdee, J. C. Scaiano, and R. Sinta, *Chem. Mater.* **8**, 2654 (1996).
- ⁸G. Pohlers, J. C. Scaiano, and R. Sinta, *Chem. Mater.* **9**, 3222 (1997).
- ⁹M. Padmanaban, H. Endo, Y. Inoguchi, Y. Kinoshita, T. Kudo, S. Masuda, Y. Nakajima, and G. Pawlowski, *Proc. SPIE* **1672**, 141 (1992).
- ¹⁰O. Suga, H. Yamaguchi, and S. Okazaki, *Microelectron. Eng.* **13**, 65 (1991).
- ¹¹S. A. MacDonald, *et al.* *Proc. SPIE* **1466**, 2 (1991).
- ¹²T. H. Fedynyshyn, M. F. Cronin, L. C. Poli, and C. Kondek, *J. Vac. Sci. Technol. B* **8**, 1454 (1990).
- ¹³P. M. Dentinger and J. W. Taylor, *J. Vac. Sci. Technol. B* **15**, 2632 (1997).
- ¹⁴C. J. Gamsky, P. M. Dentinger, G. R. Howes, and J. W. Taylor, *Proc. SPIE* **2438**, 143 (1995).
- ¹⁵T. H. Fedynyshyn, M. F. Cronin, and C. R. Szmanda, *J. Vac. Sci. Technol. B* **9**, 3380 (1991).
- ¹⁶P. M. Dentinger, K. G. Knapp, G. W. Reynolds, T. H. Fedynyshyn, and T. A. Richardson, *Proc. SPIE* **3331**, 568 (1998).
- ¹⁷T. H. Fedynyshyn, M. F. Cronin, and J. W. Thackeray, *Proc. SPIE* **1924**, 63 (1993).
- ¹⁸S. J. Bukofsky and R. D. Grober, *Appl. Phys. Lett.* **71**, 2749 (1997).
- ¹⁹P. M. Dentinger and J. W. Taylor, *J. Vac. Sci. Technol. B* (these proceedings).
- ²⁰S. J. Bukofsky, G. D. Feke, Q. Wu, R. D. Grober, P. M. Dentinger, and J. W. Taylor, *Appl. Phys. Lett.* **73**, 408 (1998).
- ²¹P. M. Dentinger, Ph.D. dissertation, University of Wisconsin–Madison, 1998.
- ²²A. Bruns, H. Luethje, F. A. Vollenbroek, and E. J. Spiertz, *Microelectron. Eng.* **6**, 467 (1987).
- ²³E. A. Kocsis and G. Zador, *Z. Anal. Chem.* **42**, 142 (1942).
- ²⁴J. E. Whitaker, R. P. Haugland, D. Ryan, P. C. Hewitt, R. P. Haugland, and F. G. Prendergast, *Anal. Biochem.* **207**, 267 (1992).
- ²⁵M. T. Z. Spence, *Handbook of Fluorescent Probes and Research Chemicals*, 6th ed., edited by R. P. Haugland (Molecular Probes, Inc., Eugene, OR, 1996), p. 679.
- ²⁶C. Eckes, G. Pawlowski, K. Pryzbilla, W. Meier, M. Madore, and R. Dammel, *Proc. SPIE* **1466**, 394 (1991).